Co-simulation-based probabilistic seismic hazard assessment method combining earthquake-event and ground-motion simulation

Shaoqing Wang[1,*], Jun Miao[2], Cuiran Zhang[1]

[1]Earthquake Engineering Research Center, China Institute of Water Resources and Hydropower Research, Beijing, 100048, China
[2]PowerChina Guiyang Engineering Corporation Limited, 550081, Guiyang, China

*Corresponding author's Email:wangsq@iwhr.com

Abstract. Accurate estimation of ground-motion intensity is the key factor in probabilistic seismic hazard analysis (PSHA) at near-fault area. To get PSHA results matched with specific geological conditions near sites, we first propose a co-simulation-based PSHA method combining event-based PSHA and stochastic finite fault method to simulate earthquake event and then ground motion in one framework. Then, we compare the PGA distribution between stochastic finite fault simulation and ground-motion prediction equations (GMPEs). Finally, we investigate the difference of hazard curve between our new method and traditional PSHA. The results show: (1) the distribution of PGAs by stochastic finite fault method is reasonable compared to GMPEs; (2) regardless of site location and investigation time, simulation-based PSHA gives identical results to traditional PSHA; (3) the new proposed co-simulation-based method can produce roughly equivalent hazard results to traditional PSHA. The results of this study can facilitate the PSHA at near-fault areas with insufficient strong-motion records.

Keywords: Event-based PSHA, stochastic finite fault method, ground-motion simulation

1 Introduction

In the seismic design of important structures such as high concrete dams, it is nowadays broadly accepted that the reliability depends on whether the input motion could accurately represent the expected seismic actions. To determine the seismic input of crucial structures, the first is to determine its intensity according to seismic hazard assessment. Probabilistic seismic hazard assessment (PSHA) was first established in the 1960s by Esteva (1963) and Cornell (1968) [1–3], and aims to estimate the probability that a ground motion intensity level will be exceeded during a future time interval combining seismicity and ground-motion prediction around a specific site. In this case, whether the predicted ground motion can represent the corresponding earthquake geologic

© The Author(s) 2024
G. Zhao et al. (eds.), *Proceedings of the 2023 5th International Conference on Civil Architecture and Urban Engineering (ICCAUE 2023)*, Atlantis Highlights in Engineering 25,
https://doi.org/10.2991/978-94-6463-372-6_4

conditions around the site is key to the final results. Thus, it is important to accurately estimate the ground motion intensity for the seismic design of important structures.

Traditional PSHA uses ground motion prediction equations (GMPEs) to determine the ground motion intensity given earthquake source mechanics (magnitude, strike, dip, etc.), source-site distances and site conditions. Many GMPEs have been developed in different countries and regions[4]. However, the strong motion records required for developing GMPEs are still sparse in China, especially in plateau and canyon regions. If the geological condition near the site is significantly different to recorded strong motions, directly using current GMPEs are not reasonable. Moreover, the lack of near-fault record makes the GMPE unreliable in areas with very short distances to earthquake faults (e.g., less than 10 km). Therefore, how to estimate the intensity of near-fault ground motion corresponding to specific geological conditions is a key problem to more realistic PSHA.

Obtaining near-fault strong motion by simulation if one of the methods to solve this problem. For example, Chiou and Young uses simulated ground motion as supplements to strong-motion database [5]. Tarbali et al. calculate the seismic hazard in New Zealand by direct simulation method [6]. However, adding simulated motion directly in strong motion databases ignores the conditions of specific site. Azar et al. propsed a stochastic ground motion simulation method and apply it into PSHA [7]. But this method cannot represent the rupture process of fault. On the other hand, as a semi-empirical method, stochastic finite fault method can not only incorperate the rupture process in the simulation, but also be very efficient, which is an effective tools for near-fault ground-motion simulation.

The objective of this papar is to obtain probabilistic hazard curves by replacing GMPEs with ground-motion intensity measure (IM) simulated by stocastic finite fault method, which can better represent real geological conditions around the site. Therefore, we first develop a co-simulation-based PSHA method combining simulation-based (or event-based) PSHA and stochastic finite fault method to simulate earthquake event and then ground motion in one framework. In this method, we consider the uncertainties of earthquake source, site conditions and path attenuation. Then, we show a comparison example between PGAs from stochastic finite fault simulation and NGA west2 GMPEs. Finally, we show the influence of replacing GMPEs to stochastic-finite-fault simulated IMs on the results of hazard.

2 Co-simulation-based PSHA combining event-based PSHA and stochastic finite fault simulation

2.1 Probabilistic seismic hazard assessment (PSHA)

Assuming a site is located on $\mathbf{s_i}$, the earthquake sources around are $\mathbf{S}$, and the recurrence of earthquakes in the study area is a stable Poisson process with an annual rate of λ, then the annual rate $\lambda_E(\mathrm{IM} > x)$ of ground motion IM exceeding x is,

$$\lambda_E(\mathrm{IM} > x) = \int_{M_t}^{M_{\max}} \int_{\mathbf{S}} \lambda f_m(m) P(\mathrm{IM} > x | m, |\mathbf{s} - \mathbf{s_i}|) \mathrm{d}\mathbf{s}\mathrm{d}m \tag{1}$$

where M_{max} and M_t are the maximum and threshold magnitudes; and $P[\mathrm{IM} > x|(m, |\mathbf{s} - \mathbf{s_i}|)]$ is the probability that an IM exceeds x given magnitude m and distance $|\mathbf{s} - \mathbf{s_i}|$. If adopting a truncated form of Gutenberg-Richter (G-R) law [8], the probability density function (p.d.f.) of magnitude can be represented as:

$$f_m(m) = \frac{\beta \exp[-\beta(m - M_t)]}{1 - \exp(M_{max} - M_t)} \tag{2}$$

where $\beta = b\log(10)$ is the model parameter.

2.2 PSHA based on co-simulation of earthquake events and ground motion.

2.2.1 Simulation-based PSHA. In engineering practice, we care about not only the annual rate of exceedance (whose reciprocal is the recurrence period), but also the probability of exceedance in certain investigation time (e.g., 50 years or 100 years). If we assume that the recurrence of earthquake follows Poisson assumption, we can calculate the probability of exceedance in investigation time T as:

$$P_T(\mathrm{IM} > x) = 1 - \mathrm{e}^{-\lambda(\mathrm{IM} > x)T} \tag{3}$$

However, if non-Poisson seismicity models, such as epidemic-type-aftershock-sequence (ETAS) model [9], STEP model [10] are adopted, Equation 3 is then not proper. Moreover, if much more types of uncertainties (not only the uncertainty of earthquake magnitude and position) are considered, the efficiency of Equation (1) will be slow down. Thus, we can obtain the hazard by event-based or simulation-based method [11–14].

If an earthquake catalog with duration T_c is simulated, the annual exceedance rate of ground motion IM at a site is:

$$\lambda_{annual}(\mathrm{IM} > x) = \frac{N_{e,all}}{T_c} \tag{4}$$

where $N_{e,all}$ is number of all earthquakes whose IMs exceed level x in the catalog. dividing the catalog into N_w windows with durations equal to the investigation time T (e.g., 50 years, 100 years, etc.), the probability of exceedances is:

$$P_T(\mathrm{IM} > x) = \frac{N_{w,e}}{N_w} \tag{5}$$

where $N_{w,e}$ is the number of catalog windows with at least one earthquake that generate IMs exceeding x.

2.2.2 Stochastic finite fault method. In engineering practice, stochastic finite fault simulation has two extinctive advantages, that is, first, it can incorporate the main source features of near-site strong earthquakes; second, it has high numerical efficiency compared with physic-based method such as finite difference method and spectral element method[15–18].

The main framework of stochastic finite fault method is described as following.

First, divide the entire rupture of earthquake into $nl * nw$ sub-faults. Every small sub-fault can then be treated as a point source. Finally, we can superposition ground motion generated by all sub-faults according to their sequences considering the rupture and propagation process, that is:

$$a(t) = \Sigma_{i=1}^{nl} \Sigma_{j=1}^{nw} a_{i_j}(t + \Delta t_{ij}) \tag{6}$$

where Δt_{ij} is the lag of time of sub-fault (i, j) compared to the rupture starting point; a_{ij} is the ground motion at site generated by sub-fault (i, j), which is obtained from a stochastic Fourier-spectrum-based method. We can get the Fourier spectral amplitude of sub-fault $|A_{ij}(f)|$ from a product of Brune source spectrum $S_{ij}(f)$, path attenuation $P_{ij}(f)$, and site effect coefficient $G_{ij}(f)$:

$$|A_{ij}(f)| = S_{ij}(f) \cdot P_{ij}(f) \cdot G_{ij}(f) \tag{7}$$

The most widely adopted source spectrum is the dynamic corner frequency mode [19], that is:

$$S_{ij}(f) = \frac{CM_{0ij}H_{ij}(2\pi f)^2}{1+\left(\frac{f}{f_{cij}}\right)^2} \tag{8}$$

where C is a constant related to radiation pattern, free surface effect, partition onto horizontal components, density, and shear-wave velocity. M_{0ij} is the seismic moment of sub-fault in dyne cm. H_{ij} is a scaler factor and $f_{0_{ij}}$ is the corner frequency obtained as follows.

$$f_{cij} = 4.9 \times 10^6 N_{Rij}^{-\frac{1}{3}} V_s \left(\frac{\Delta\sigma}{M_{0\text{ave}}}\right)^{\frac{1}{3}} \tag{9}$$

where N_{Rij} is number of ruptured sub-faults when the rupture front arrives at sub-fault (i, j), V_s is shear wave velocity, and $\Delta\sigma$ is stress drop. $M_{0\text{ave}}$ is the average seismic moment over the entire rupture.

The path attenuation $P_{ij}(f)$ can be calculated as:

$$P_{ij}(f) = \frac{\exp\left(-\frac{\pi f R_{ij}}{QV_s}\right)}{R_{ij}} \tag{10}$$

where R_{ij} is the distance from sub-fault to the site. $Q = Q_0 f^{\eta}$ is a frequency-dependent attenuation factor in which Q_0 is the factor at $f = 1$ Hz.

The site effect coefficient $G_{ij}(f)$ can be calculated as:

$$G_{ij}(f) = \exp(-\pi\kappa f) \tag{11}$$

which is a high-cut filter to model near- surface “kappa” effects.

2.2.3 PSHA based on simulated ground motion IMs. The key of applying ground motion IMs simulated by stochastic finite-fault method is the conditional probability term in Equation (1), that is, $P(\mathrm{IM} > x|m, |\mathbf{s} - \mathbf{s_i}|)$. Due to the complexity of earthquake source, propagation media and site condition, we cannot obtain reasonable conditional probability if we do not incorporate all uncertainties in stochastic finite fault method. The new PSHA method proposed in this paper considers all uncertainties to calculate the hazard curve combining simulated ground-motion IMs by stochastic finite fault method and event-based PSHA. The main steps are as follows:

Step 1: Determine the source-related parameters around the site, including locations of possible ruptures, source mechanisms, and seismicity parameters (annual rates and b value of G-R law).

Step 2: Simulate an earthquake catalog with enough time duration based on the parameters determined by step 1 (including locations, magnitudes, event time of every earthquake).

Step 3: Determine the parameter distributions of stochastic finite fault method according to the simulated catalog and geological conditions in the study area.

Step 4: Simulate the ground motion of each earthquake in the simulated catalog and calculate the ground motion IMs. Calculate the hazard curve based on Equations (4) and (5).

The difficulty in applying the forementioned steps is how to determine the parameter distributions of stochastic finite fault method (Step 3). Because we do not intend to simulate the hazard curve for a real region, and we plan to compare our results with traditional PSHA, we in this paper use global parameters as far as possible. Here, we consider five types of uncertainties, of which the first four of them are single parameter, listed in Table 1 and described as follows.

1)Rupture length L. We assume a logarithmic normal distribution of this parameter with logarithmic mean $\log_{10}(L) = -2.57 + 0.62M$ and standard deviation 0.15 according to Wells and Coppersmith [20].

2)Stress drop $\Delta\sigma$. We also assume a logarithmic normal distribution of stress drop. Allmann and Shearer proposed that global stress drop is in the range of 3~500 Bar with an average of 30~40 Bar [21]. However, strike-fault earthquakes tend to have highest stress drop with an average of 100 Bar. According to their database, we use a stress drop distribution with mean 100 Bar and logarithmic standard 0.642. The distribution is truncated into a range of 3~500 Bar.

3)High frequency attenuation coefficient κ_0, We assume κ_0 follows normal distribution. Lang et al. summerizes some research on κ_0 and derives that κ_0 is negtively correlated with $\log(Vs_{30})$ [22]. According to that study, we use a κ_0 distribution with a mean of 0.0335 and standard deviation of 0.0141 assuming $Vs_{30} = 700{\sim}800\ \mathrm{m/s}$.

4)Attenuation coefficient Q_0 and η. We assume they all follows even distribution. Considered that NGA GMPEs are mainly based on records from California, we use $Q_0 = 250{\sim}300$ and $\eta = 0.4{\sim}0.5$ according to the results of California by Baqer and Mitchell [23].

5)Rupture slip distribution. In stochasitc finite fault method, uneven slip distribution can be used to assign the seismic moment of each sub-fault. In real rupture process,

strong motions are mainly related to the slip herogeneity inside the rupture. In this study, we uses the slip distribtuion recipe from Irikura and Miyake [24]. To consider every possibility we use three types of asperities, as shown in Figure 1, and assume every type has identical possibility.

Table 1. Parameter distribution in stochastic finite fault simulation

Parameter name	Distribution type	Mean	Standard deviation	Parameter range
Rupture length L	Logarithmic normal	$\log_{10}(L) = -2.57 + 0.62M$	0.15	~
Stress drop σ	Logarithmic normal	100 Bar	0.642	3~500 Bar
High cut-off parameter κ_0	Normal	0.03348	0.01411	0.013~0.0711
Attenuation parameter Q_0	Normal	~	~	250~300
Attenuation parameter η	Normal	~	~	0.4~0.5

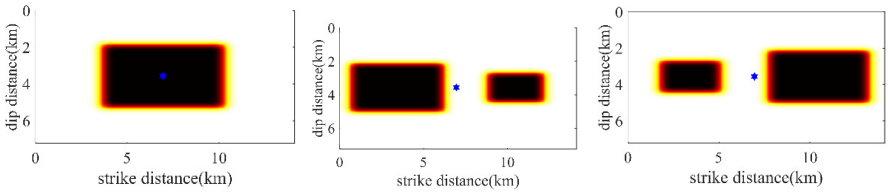

Fig. 1. Location of asperities

3 Comparison of simulated IMs with GMPEs

To ensure the reasonability of simulated hazard, we first compare the simulated ground motion IMs with GMPEs in this section. Because NGA GMPEs [25–29] use global records, we also use global parameters in Table 1 for stochastic ground motion simulation. We use magnitude from M5 to M8 and rupture distances from 10 km to 30 km with an interval of 1 km. The rupture is set as strike slip with a dip of 90 degree. We simulate 500 times for each combination of magnitude and rupture distance. The parameter of each simulation is randomly sampled from the distributions described in Table 1and the rupture slip pattern of each simulation is randomly sampled from Figure 1.

Figure 2 shows the comparison of PGA distribution between simulations and NGA GMPEs with four different magnitudes. Figures 2a~d show the results of PGA mean. First, for M5~M7, simulated PGA means by stochastic finite fault method is similar to the mean from five NGA GMPEs. But for M8, stochastic finite fault simulation

produces lower PGAs compared to NGA GMPEs. This may be caused by larger rupture area and spread energy. Moreover, when the rupture distance is larger, PGAs from simulation becomes larger than NGA GMPEs. This may be the result of an unreasonable Q_0 and η. Figures 2e~f show the comparison of standard deviations between both simulations and GMPEs. We can see that regardless of magnitudes and rupture distances, stochastic finite fault simulations always produce larger uncertainty than GMPEs.

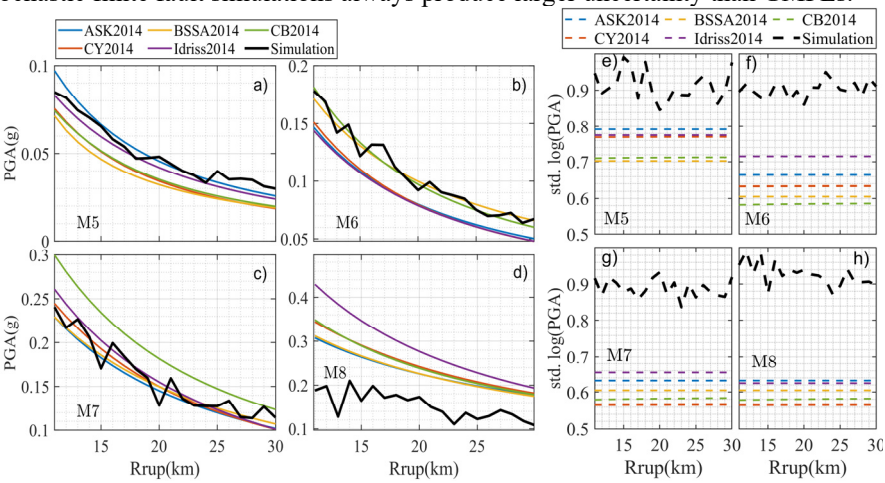

Fig. 2. PGA mean (a~d) and standard deviation (e~f) between stochastic finite fault simulation and NGA GMPEs for M5~M8.

4 Near-fault hazard based on co-simulation of earthquake events and ground motion

4.1 Design of scenario

To compare the results of proposed co-simulation-based PSHA and traditional PSHA, we set an engineering scenario as follows. First, we assume a 160*40 km square as potential source area, shown in Figure 3, around which we choose three sites A, B and C as our research objects. Among those, site A is inside the potential source area; sites B and C are outside, with a minimum distance of 5 km to the source area, as the black triangles show in Figure 3. We choose $Vs_{30} = 760\ \mathrm{m/s}$ for all three sites. The earthquakes around are crustal earthquakes. The results of Section 3 show stochastic finite fault simulations will underestimate PGA for M8 than GMPEs. Thus, in this section, we choose M4 and M7 as the minimum and maximum magnitudes, respectively. The parameter of G-R law is $b = 0.85$ and annual recurrence rate of earthquake is $\lambda = 32$ times per year. We fix the strike and dip angles as both 90 degrees. We choose PGA as our interested ground-motion IM.

We set three scenarios in this section.

Scenario 1: traditional analytical PSHA. We calculate the annual rate directly using Equation (1) and probability of exceedance in 50 years directly using Equation (3). In

calculation, we use two NGA GPMEs, that is, BSSA14 and ASK2014 [25,26]. This scenario uses the same method with most of the hazard assessment in engineering practices, which can be a validation of our results.

Scenario 2: event-based PSHA using GMPE. In this scenario, we first simulate a 1-million-year catalogue, assuming that the source location of each earthquake is randomly distributed in the square source area and the dimensions of them are determined by the scaling law in Wells and Coppersmith. Then, we calculate the PGAs at sites A, B and C using BSSA2014. Finally, we calculate the annual rate of exceedance and probability of exceedance in 50 years using Equations (4) and (5). This scenario is to validate the even-based PSHA method.

Scenario 3. PSHA method based on co-simulation of both earthquake events and ground motion. In this scenario, we also use Poisson process to simulate earthquake catalog. However, due to the high demand of computer resources for ground motion simulation, we shorten the simulated catalog to 100 thousand years. Also assuming a random distributed source and scaling law in Wells and Coppersmith, we simulate ground motions and PGAs at site B for each earthquake in the catalog. In simulation, we choose parameters of stochastic finite fault method from Table1 and Figure 1. Finally, we obtain the annual rate of exceedance and probability of exceedance in 50 years using Equations (4) and (5).

In those three scenarios, Sceario I produces accurate analytic solution. While Scenarios 2 and 3 produce approximate solutions based on Monte-Carlo simulation. Figure 4 shows the earthquake rupture locations (M6~M7) in a 10-year window of earthquake catalog. Because it is difficult to show ruptures with dip of 90 degree, the ruptures in Figure 4 are accually with dip of 65 degrees only for display.

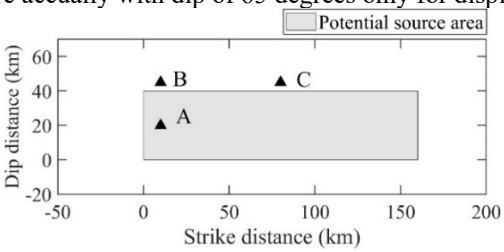

Fig. 3. Plan view of study area

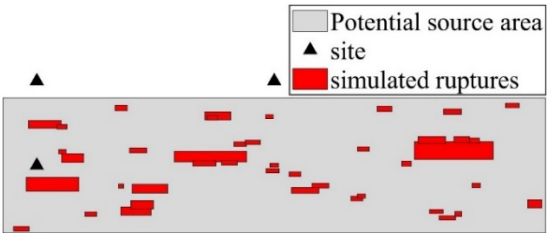

Fig. 4. Examples of simulated ruptures (a 10-year window with magnitude M6-M7 and dip of 65 degree only for display)

4.2 Results of hazard

We first compare the results of Scenarios 1 and 2 when using BSSA2014, that is, the difference between traditional analytical PSHA and event-based PSHA. Figures 5a and b show the annual exceedance rate and probability of exceedance in 50 years at sites A, B and C in Scenarios 1 and 2, respectively. It can be seen that, when the simulation duration is 1 million years, not matter the investigation time is 1 year or 50 years, event-based PSHA simulation produces identical results with traditional analytical PSHA.

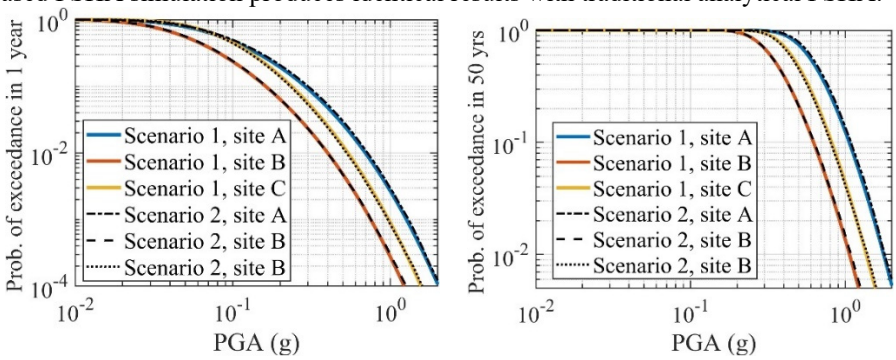

(a) annual exceedance rate (b)probability of exceedance in 50 years

Fig. 5. Hazard results of Scenarios 1 and 2.

Then, we compare the results between scenarios 3 and 1 (identical to 2), that is, the difference between proposed co-simulation-based PSHA and traditional PSHA. In this section, we calculate the hazard at site B.

Figures 6a and b show the annual exceedance rate and probability of exceedance in 50 years between Scenarios 1 (2) and 3. Because the results of scenarios 1 and 2 are identical, we only show the results of Scenarios 1 and 3. The results show, first, that compared with the traditional PSHA, the proposed co-simulation-based PSHA produces roughly equivalent hazard curves for both 1-year and 50-year investigation time. Figure 6a shows that, when the exceedance probability is relative higher (PGA less than ~0.1 g), Scenario 3 produces hazard curve similar to traditional PSHA with BSSA 2014; when the exceedance probability becomes lower (PGA=0.2~0.7 g), Scenario 3 becomes closer to the results of traditional PSHA with ASK2014; when the exceedance probability is very small, the PGA of Scenario 3 becomes lower than traditional PSHA with BSSA2014 and ASK2014. Meanwhile, Figure 6b shows that for investigation time of 50 years, when PGA<~0.7g, Scenario 3 is more closer to traditional PSHA with BSSA2014; while PGA is larger, it shows similar trends with Figure 6a. Compared with Figures2 a~d, the reason of this trend for Scenario 3 may be that, when the magnitude is moderate (M5), the PGAs by stochastic finite fault simulation are closer to ASK2014; When the magnitude is larger (M6), they are much closer to BSSA2014; When the magnitude is very large (M7~M8), they tend to be lower than both of the two GMPEs.

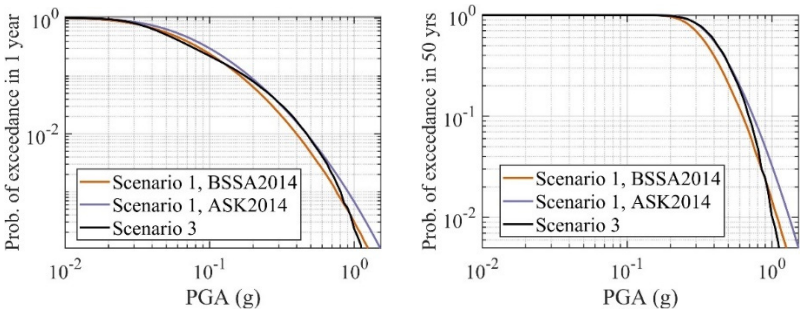

(a)Annual probability of exceedance (b)Probability of exceedance in 50 years

Fig. 6. Hazard results of scenarios 1 (2) and 3

5 Conclusion

This paper first proposes a co-simulation-based PSHA method combining event-based PSHA and stochastic finite fault method simulating earthquake event and then ground motion in one framework. Then, we compare the PGAs between stochastic finite fault simulation and NGA GMPEs. Finally, we compare the different between proposed co-simulation-based PSHA and traditional PSHA methods. The results show:

1. If adopt global parameters and set rupture slip distribution properly, PGA means simulated by stochastic finite fault method are similar to five NGA GMPEs when the magnitude is less than or equal to M7 and slightly lower when the magnitude is equal to M8. The standard deviations are relatively larger than GMPEs.
2. Regardless of site location and investigation time, event-based PSHA produces identical hazard curves to traditional analytical PSHA.
3. The proposed co-simulation-based PSHA combining earthquake events and ground motion simulation can produce roughly equivalent results of hazard compared with traditional PSHA.

Acknowledgments

This work was financially supported by the Science and Technology Project of PowerChina Guiyang Engineering Corporation Limited. (DJ-ZDXM-2021-03), Science and Technology project of Huaneng Lancang River Hydropower Inc. (HNKJ22-H108 HY2022/D), and Science and Technology Thematic Funding Project of Department of Water Resources of Guizhou Province (KT201902).

References

1. Esteva L (1963) Regionalizacion sismica de la Republica Mexicana. Rev. Soc. Mex. do Ing. Sismica, 1:31–5.
2. Cornell C A (1968) Engineering seismic risk analysis. Bull. Seismol. Soc. Am., 58:1583–606.
3. McGuire R K (2008) Probabilistic seismic hazard analysis: Early history. Earthq. Eng. Struct. Dyn., 37:329–38. https://doi.org/10.1002/eqe.765.
4. Zhang B, Yu Y, Li X, and Wang Y (2022) Ground motion prediction equation for the average horizontal component of PGA, PGV, and 5% damped acceleration response spectra at periods ranging from 0.033 to 8.0s in southwest China. Soil Dyn. Earthq. Eng., 159:107297. https://doi.org/10.1016/j.soildyn.2022.107297.
5. Chiou B S J, and Youngs R R (2014) Update of the Chiou and Youngs NGA model for the average horizontal component of peak ground motion and response spectra. Earthq. Spectra, 30:1117–53. https://doi.org/10.1193/072813EQS219M.
6. Tarbali K, Bradley B, Huang J, and Polak V (2018) New Zealand simulation-based probabilistic seismic hazard analysis. QuakeCoRE FP1 Gr. motion Simul. Valid.
7. Azar S, Dabaghi M, and Rezaeian S (2019) Probabilistic seismic hazard analysis using stochastic simulated ground motions. 13th Int. Conf. Appl. Stat. Probab. Civ. Eng. ICASP 2019, .
8. Gutenberg B, and Richter (1944) Frequency of earthquakes in California. Bull. Seismol. Soc. Am., 34:185–8.
9. Ogata Y (1988) Statistical Models for Earthquake Occurrences and Residual Analysis for Point Processes. J. Am. Stat. Assoc., 83:9–27. https: // doi. org/ 10. 1080/ 01621459. 1988. 10478560.
10. Gerstenberger M C, Wiemer S, Jones L M, and Reasenberg P A (2005) Real-time forecasts of tomorrow's earthquakes in California. Nature, 435:328–31. https: //doi. org/ 10. 1038/ nature03622.
11. Wang S, Werner M J, and Yu R (2022) How Well Does Poissonian Probabilistic Seismic Hazard Assessment (PSHA) Approximate the Simulated Hazard of Epidemic-Type Earthquake Sequences? Bull. Seismol. Soc. Am., 112:508–26. https: //doi. org/ 10. 1785/0120210022.
12. Wang S, Werner M J, and Yu R (2022) Reply to "Comment on 'How Well Does Poissonian Probabilistic Seismic Hazard Assessment (PSHA) Approximate the Simulated Hazard of Epidemic-Type Earthquake Sequences?' by Shaoqing Wang, Maximilian J. Werner, and Ruifang Yu" by Iunio Iervolino, and Massimil. Bull. Seismol. Soc. Am., 112:2762–9. https://doi.org/10.1785/0120220081.
13. De Risi R, Wang S, Werner M J, De Luca F, Vardanega P J, Pokhrel R M, et al. (2020) SIMULATION-BASED PSHA FOR THE KATHMANDU VALLEY : SENSITIVITY TO HYPOCENTRE RANDOMISATION. 17th World Conf. Earthq. Eng., Sendai,Japan: , p. 1–3.
14. Iervolino I (2019) Generalized earthquake counting processes for sequence-based hazard. Bull. Seismol. Soc. Am., 109:1435–50. https://doi.org/10.1785/0120180271.
15. Rodgers A J, Pitarka A, Anders Petersson N, Sjogreen B, McCallen D B, and Abrahamson N (2019) Broadband (0-5 Hz) fully deterministic 3D ground-motion simulations of a magnitude 7.0 Hayward fault earthquake: Comparison with empirical ground-motion models and 3D path and site effects from source normalized intensities. Seismol. Res. Lett., 90:1268–84. https://doi.org/10.1785/0220180261.

16. Molnar S, Cassidy J F, Olsen K B, Dosso S E, and He J (2014) Earthquake ground motion and 3D Georgia basin amplification in Southwest British Columbia: Deep Juan de Fuca Plate scenario earthquakes. Bull. Seismol. Soc. Am., 104:301–20. https: //doi. org/ 10. 1785/ 0120110277.
17. He C H, Wang J T, Zhang C H, and Jin F (2015) Simulation of broadband seismic ground motions at dam canyons by using a deterministic numerical approach. Soil Dyn. Earthq. Eng., 76:136–44. https://doi.org/10.1016/j.soildyn.2014.12.004.
18. Wang X C, Wang J T, Zhang L, Li S, and Zhang C H (2021) A multidimension source model for generating broadband ground motions with deterministic 3d numerical simulations. Bull. Seismol. Soc. Am., 111:989–1013. https://doi.org/10.1785/0120200221.
19. Motazedian D, and Atkinson G M (2005) Stochastic finite-fault modeling based on a dynamic corner frequency. Bull. Seismol. Soc. Am., 95:995–1010. https: //doi. org/ 10. 1785/0120030207.
20. Wells D L, and Coppersmith K J (1994) New empirical relationships among magnitude, rupture length, rupture width, rupture area, and surface displacement. Bull. - Seismol. Soc. Am., 84:974–1002.
21. Allmann B P, and Shearer P M (2009) Global variations of stress drop for moderate to large earthquakes. J. Geophys. Res. Solid Earth, 114:1–22. https: // doi. org/ 10. 1029/ 2008JB005821.
22. Ziping L, Ruifang Y, Liang X, Lei F, and Jian Z (2022) An estimation model of high frequency attenuation coefficient of ground motion for local site. Acta Seismol. Sin., 44:1–10.
23. Baqer S, and Mitchell B J (1998) Regional variation of Lg coda Q in the continental United States and its relation to crustal structure and evolution. Pure Appl. Geophys., 153:613–38. https://doi.org/10.1007/978-3-0348-8711-3_17.
24. Irikura K, and Miyake H (2011) Recipe for predicting strong ground motion from crustal earthquake scenarios. Pure Appl. Geophys., 168:85–104. https://doi.org/10.1007/s00024-010-0150-9.
25. Abrahamson N A, Silva W J, and Kamai R (2014) Summary of the ASK14 ground motion relation for active crustal regions. Earthq. Spectra, 30:1025–55. https: //doi. org/ 10. 1193 /070913EQS198M.
26. Boore D M, Stewart J P, Seyhan E, and Atkinson G M (2014) NGA-West2 equations for predicting PGA, PGV, and 5% damped PSA for shallow crustal earthquakes. Earthq. Spectra, 30:1057–85. https://doi.org/10.1193/070113EQS184M.
27. Chiou B S J, and Youngs R R (2014) Update of the Chiou and Youngs NGA model for the average horizontal component of peak ground motion and response spectra. Earthq. Spectra, 30:1117–53. https://doi.org/10.1193/072813EQS219M.
28. Campbell K W, and Bozorgnia Y (2014) NGA-West2 ground motion model for the average horizontal components of PGA, PGV, and 5% damped linear acceleration response spectra. Earthq. Spectra, 30:1087–114. https://doi.org/10.1193/062913EQS175M.
29. Idriss I M (2014) An NGA-West2 Empirical Model for Estimating the Horizontal Spectral Values Generated by Shallow Crustal Earthquakes. Earthq. Spectra, 30:1155–77. https: //doi.org/10.1193/070613EQS195M.

Open Access This chapter is licensed under the terms of the Creative Commons Attribution-NonCommercial 4.0 International License (http://creativecommons.org/licenses/by-nc/4.0/), which permits any noncommercial use, sharing, adaptation, distribution and reproduction in any medium or format, as long as you give appropriate credit to the original author(s) and the source, provide a link to the Creative Commons license and indicate if changes were made.

The images or other third party material in this chapter are included in the chapter's Creative Commons license, unless indicated otherwise in a credit line to the material. If material is not included in the chapter's Creative Commons license and your intended use is not permitted by statutory regulation or exceeds the permitted use, you will need to obtain permission directly from the copyright holder.